Contents lists available at SciVerse ScienceDirect

Physica B

Enhanced low-field-magnetoresistance and electro-magnetic behavior of $La_{0.7}Sr_{0.3}MnO_3/BaTiO_3$ composites

P.T. Phong [a,b,*], D.H. Manh [c], N.V. Dang [d], L.V. Hong [c], I.J. Lee [a]

[a] Department of Nanomaterial Chemistry, Dongguk University, 707 Suckjang-dong, Gyeongju-Si, Gyeonbuk 780-714, Korea
[b] Nha Trang Pedagogic College, 01 Nguyen Chanh Street, Nha Trang City, Khanh Hoa Province, Viet Nam
[c] Institute of Materials Science, Vietnam Academy of Science and Technology, 18 Hoang Quoc Viet Road, Cau Giay District, Ha Noi, Viet Nam
[d] College of Science, Thai Nguyen University, Thai Nguyen City, Viet Nam

ARTICLE INFO

ABSTRACT

We report the structural, magentoresistance and electro-magnetic properties of ferromagnet–ferroelectric–type $(1-x)La_{0.7}Sr_{0.3}MnO_3/xBaTiO_3$ (with $x=0.0\%$, 3.0%, 6.0%, 12%, 15.0% and 18.0%, in wt%) composites fabricated through a solid-state reaction method combined with a high energy milling method. The insulator–metal transition temperature shifts to a lower temperature and resistivity increases while the feromagnetic–paramagnetic transition temperature remains almost unchanged with the increase of $BaTiO_3$ content. Magnetoresistance of the composites at an applied magnetic field $H=3$ kOe is enhanced in the wide temperature ranges with the introduction of $BaTiO_3$, which could be explained by the enhanced spin polarized tunneling effect induced by the introduction of $BaTiO_3$. The low-field magnetoresistance of the composite is analyzed in the light of a phenomenological model based on the spin polarized tunneling at the grain boundaries. Furthermore, the temperature dependence of resistivity for this series has been best-fitted by using the adiabatic small polaron and variable range hopping models. These models may be used to explain effect of BTO on the electronic transport properties on high temperature paramagnetic insulating region.

1. Introduction

The discovery of colossal magnetoresistance (CMR) effect in doped manganites $R_{1-x}A_xMnO_3$ (R=rare earth, A=Ca, Sr, Ba...) have renewed interests in the study of these materials. So far, two CMR effects have been found in these manganites, that is, the intrinsic CMR and extrinsic CMR. The intrinsic CMR is maximized near the the Curie temperature (T_C). According to Zener [1], the double exchange (DE) mechanism is useful to explain the CMR phenomena observed near the T_C at a relatively high magnetic field (up to several kOe). The extrinsic CMR, which is related to the grain boundaries (both natural as well as artificial), can be explained by spin polarized tunneling [2] or spin dependent scattering [3]. Nowadays, research focuses on how to obtain a large value of the MR at a low field and room temperature in order to satisfy practical applications. Many attempts have been made to improve the low field magnetoresistance (LFMR) effect of manganites by making a composite manganites materials with secondary phases such as insulator [4–8], magnetic materials

[9–11], or metals [12–15]. Most of these studies mainly focused on the influence of artificial grain boundaries on electro-magnetic behavior and enhanced LFMR in composites. Recently, the LFMR properties of $La_{0.7}Ca_{0.3}MnO_3/BaTiO_3$ (LCMO/BTO) were investigated [16–18]. Esa et al. [16] observed that grain boundary layer $BaTiO_3$ decreases the ferro–para/metal–insulator transition temperatures (T_C, T_{MI}) of LCMO/BTO composites, while it increases LFMR. In order to explain the enhancement of MR, they invoke the magnetoelectric coupling associated with the magnetostrictive LCMO and piezoelectric perovskite BTO. Similarly, Sunita Keshri (Shaw) et al. [17] reported the decrease in insulator–metal transition temperature (T_{MI}) for LCMO/BTO composites with the increase of BTO concentration and observed a double peak behavior of $\rho-T$ curves for the entire series. Conversely, Ren et al. [18] presented that the T_{MI} shifts to higher temperature and the resistivity decreases with the increase of low content BTO in LCMO/BTO. Magnetoresistance (MR) of the composites is enhanced over the whole temperature range as a result of the introduction of BTO. By calculating in terms of a ferromagnetic grain coupling model, they attribute these transport properties to the enhancement of the ferromagnetic coupling between the neighboring grains, which could be explained by the increase of the carrier concentration at the grain boundary due to the introduction of BTO and the associated magnetoelectric coupling

* Corresponding author at: Department of Nanomaterial Chemistry, Dongguk University, 707 Suckjang-dong, Gyeongju-Si, Gyeonbuk 780-714, Korea. Tel./fax: +82 54 770 2220.
E-mail address: ptphong.nh@khanhhoa.edu.vn (P.T. Phong).

effect. For the comparison point of view and to avoid decline in T_C, we synthesized $La_{0.7}Sr_{0.3}MnO_3/BaTiO_3$ (LSMO/BTO) composites by the solid state reaction method combined with the high energy milling method. Then, their structural, low-field magnetoresistance and electro-magnetic properties of LSMO/BTO have been studied. Furthermore, we utilizes a phenomenological model based on the spin polarized tunneling to explain LFMR characteristic and systematically investigated the effect of BTO on the electrical property using different models. We believe that this research can provide valuable information regarding on the effects of BTO on electro-transport and magnetic property of LSMO/BTO. In addition, we also found that enhanced room temperature low-field magnetoresistance accompanying effect of grain boundary on the spin polarized tunneling, and deduced the parameters of conductivity characteristics using the adiabatic small polaron and variable range hopping models, which was not found before.

2. Experimental

These $(1-x)La_{0.7}Sr_{0.3}MnO_3/xBaTiO_3$ ($x=0$; 0.03; 0.06; 0.12; 0.15; 0.18) composites were prepared by three steps. First, the LSMO powder was synthesized by a conventional solid state reaction method combined with a high energy milling method. High purity (99.99%) La_2O_3, $SrCO_3$ and MnO powders were mixed in the appropriate stoichiometric ratio and ground. The well-mixed powders were preheated at a temperature of 1250 °C for 15 h. Subsequently, it was heated at 1300 °C for 10 h. $BaTiO_3$ powders were also prepared by the solid state reaction method by taking stoichiometric amounts of $BaCO_3$ and TiO_2 as starting materials. The mixture powders were sintered at 1300 °C for 5 h. Next, the LSMO and BTO powders were ground by an energy milling machine for 7 h. Finally, the appropriate amount of LSMO

Fig. 1. Powder X-ray diffraction patterns for pure LSMO, BTO and LSMO/BTO composites.

powders and BTO powder were mixed and a homogenous powder was pressed in pellets at pressure of 10 MPa/cm² and sintered at 900 °C for 4 h. The structural characterization has been done by employing the X-ray diffraction (XRD) technique at room temperature in the 2θ range of 20°–80° with a step size of 0.03° using $CuK\alpha$ radiation and the surface morphology was observed by scanning electron microscopy (SEM). The magnetizations of these samples were measured by a Vibrating Sample Magnetometer (VSM) in the temperature range of (100–400 K). The electrical transport behaviors were measured by standard four-probe method in the temperature range from 50 to 320 K for all samples using a Keithley 2000 and 2001 digital multimeters. A magnetic field of 3 kOe was applied to measure the MR effect.

3. Results and discussion

Fig. 1 shows the XRD spectra of all the samples including pure LSMO, pure BTO and LSMO/BTO composites. The peaks of LSMO and BTO are indicated by (∗) and (¤) in this figure, respectively. At low doping level ($x \leq 0.06$), it is hard to observe the peaks related to BTO. However, the peaks related to BTO clearly evolve when x is greater than 0.6. Furthermore, the peaks related to LSMO show no shift with the addition of BTO. These combined results indicate that no chemical reaction occurs between LSMO and BTO phases and LSMO and BTO phases coexist.

The representative SEM micrographs of LSMO/BTO composites are shown in Fig. 2. It can be seen that the grain size of pure LSMO is around 1 μm. Esa et al. [16] and Sunita Keshri (Shaw) et al. [17] reported that microstructure of the composites are found to be significantly different from that of the parent sample due to the strain induced by the presence of BTO grains. BTO being both ferroelectric and piezoelectric could have additional strain at the grain boundary of LSMO. The induced strain in the composites can be also explained using the size distribution of grains. Smaller grains have higher surface tension and this act in the same manner as hydrostatic pressure. This fact suggests that the quadratic gradient may exist between the surface and the bulk of grains leading to strain in the microstructure.

The temperature dependent magnetization for composites measured in an applied magnetic field of 100 Oe, is plotted in Fig. 3. By taking the derivative dM/dT, T_C was estimated at 357 K for the all studied samples. This is due to the fact that the PM–FM phase transition is an intrinsic and intragrain property. The observed constancy of T_C also indicates that stoichiometry of LSMO phase within the grains remains essentially unchanged. This result implies that as BTO is not accommodated within the perovskite structure but occupies only at the grain boundaries of LSMO grains.

The field dependence of magnetization curves at 300 K from 0 to 10 kOe for the LCMO/BTO composite is shown in Fig. 4. The M–H curve indicates that the magnetization of the samples
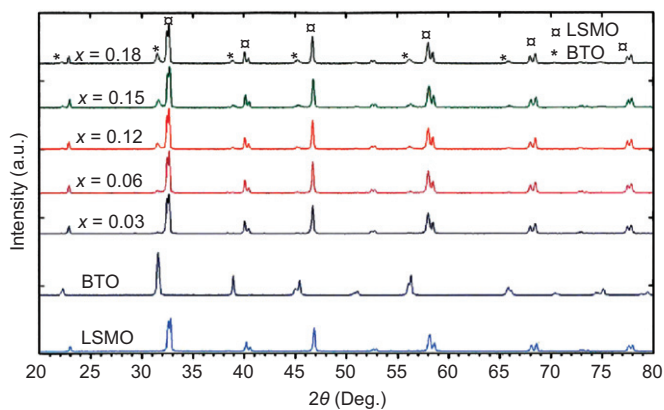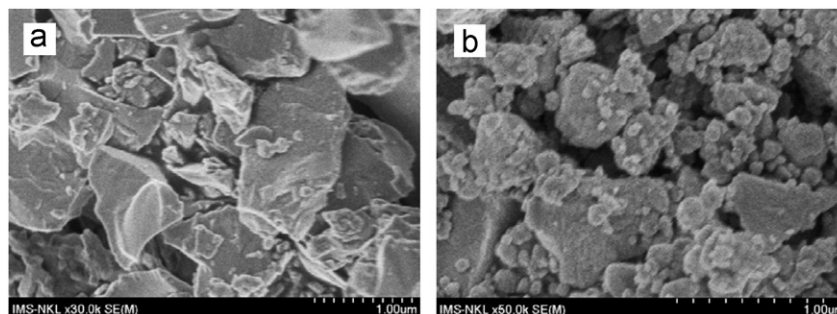

Fig. 2. The SEM photographs for LSMO/BTO composites, (a) $x=0$ and (b) $x=0.18$.

increases rapidly at low fields and then tends to saturate at higher field. The value of the magnetization of the composites decreases with x because of the reduced volume fraction of LSMO phase and extra magnetic disorder originating from BTO content. These demonstrate that the ferromagnetic order is weakened with the BTO content while magnetic disorder increases. Thus, the inclusion of ferroelectric BTO dilutes the magnetization of composite samples. The magnetization decreases almost linearly with BTO concentrations (x) as shown in the inset of Fig. 4.
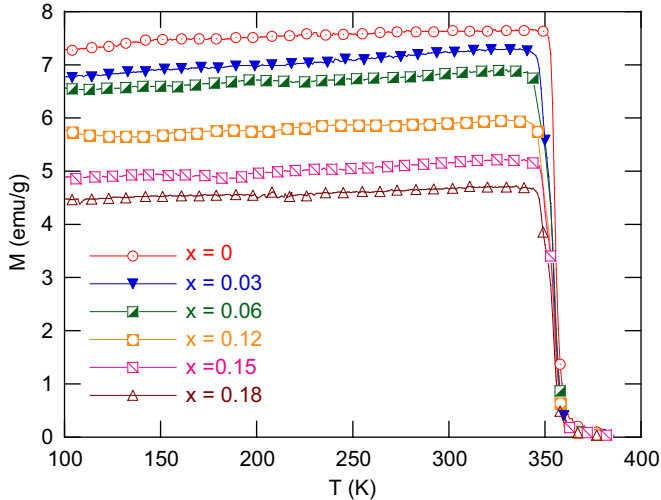

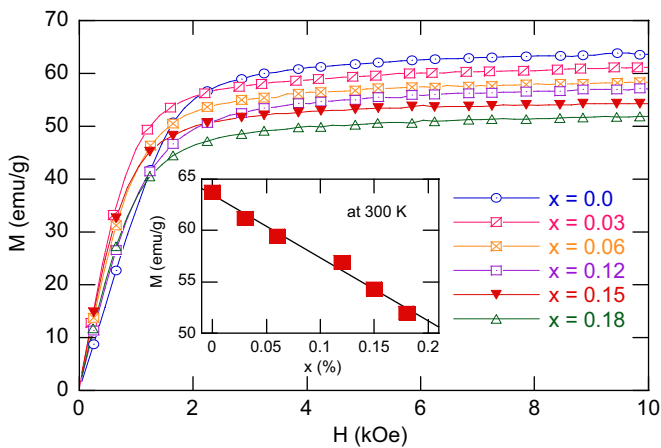**Fig. 3.** $M_{ZFC}(T)$ at 100 Oe for LSMO/BTO composite samples.

Fig. 4. $M(H)$ at 300 K for LSMO/BTO composite samples in magnetic field (0–10 kOe). The inset shows the plot of magnetization vs. BTO content.
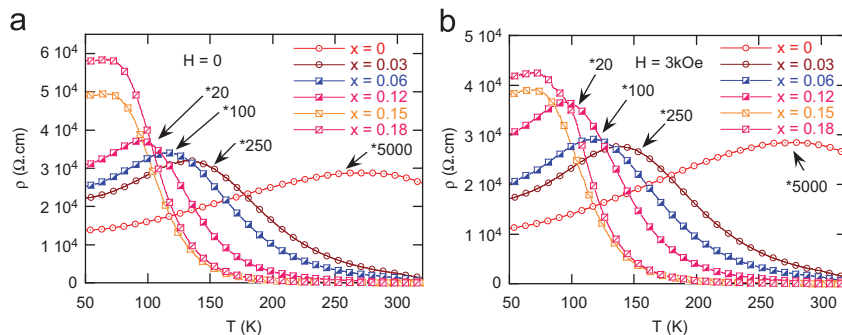
Fig. 5 shows the temperature dependence of the resistivity for the LSMO/BTO composites with different BTO content, measured within a temperature range of 50–320 K without and with magnetic field $H=3$ kOe. All the composites showed a distinct metal-insulator transition. The T_{MI} decreases from 295 K for $x=0$ to 51 K, for $x=0.18$. It is clear that the resistivity of all composites is greater than of the pure LSMO and their T_{MI} shifts down to a lower temperature. The strong depression of the T_{MI} could be caused by the induced lattice disorder and also by the increased fraction of ferroelectric BTO phase. This also causes an increase in the carrier scattering leading to a corresponding enhancement in the resistivity. Since BTO behaves as a ferroelectric, the LSMO/BTO composites are similar to the ferromagnet/insulator type composites. Large numbers of interfaces and boundaries between LSMO and BTO grains may act as additional barriers. This causes the increase in the carrier scattering leading to enhancement in the resistivity and hence, reduces the metallic transition temperature. However, in these composites, the resistivity of the samples does not change regularly with the grain size. Hence, it is reasonable to assume that the distribution and the connectivity of the grains play a more important role in the conduction. Otherwise, recently Ren et al. [18] reported that the resistivity of LCMO/BTO composites decreases and T_{MI} shifts to higher temperature region as the BTO content increases. Meanwhile, Sunita Keshri (Shaw) et al. [17] observed the double peak of $\rho - T$ curves in LCMO/BTO samples. That is very unlikely and totally contrary to our results. According to Esa et al. [16], BTO grains present at the grain boundary of the LCMO grains cannot generate charges at the grain surface. The reason is that a net dipole moment or spontaneous polarization is normally unexpected in such magneto-ferroelectric composites in the absence of such external electric field because the surface charges are rapidly neutralized by ambient charged particles. On the other hand, as seen in Fig. 5, the resistivity of our samples is much larger than those of same materials use in Ref. [16–18]. Resistivity of the sample with $x=0.18$ is 8 orders of magnitude larger than that of the sample with $x=0$. This may be due to the nature of BTO. In pure LSMO, the electrical transport is achieved through a direct contact between LSMO grains. However, in BTO-doped composites, there are two kinds of conduction channels connected parallel to each other [19,20]. One is related to LSMO grains, and determined the transport properties of the system through direct contact between LSMO grains. The other is related to dopant BTO. Since the dopant was mainly segregated at the grain boundaries and on the surface of LSMO, it produces energy barriers to electrical transport process, which results in the higher resistivity for the doped composites.

In order to understand the effect of BTO on the electrical transport mechanism of LSMO/BTO composites, the electrical resistivity data in $T > T_{MI}$ (with and without the application of the magnetic field) is analyzed by different models.

Fig. 5. Temperature dependence of resistivity for LSMO/BTO composites in $H=0$ (a) and $H=3$ kOe (b).

The temperature dependence of the electronic transport behavior at the high temperature ($T > T_{MI}$) region can be explained by using three different models: (i) Mott variable range hopping model (VRH) [21]. The resistivity can be expressed as $\rho = \rho_0 \exp(T_0/T)^{1/4}$ in $T_{MI} < T < \theta_D/2$, where $T_0 = 16\alpha^3/k_B N(E_F)$, k_B is Boltzmanns constant, $N(E_F)$ is the density of states at the Fermi level and θ_D is the Debye temperature [22]. In this study, we have selected α value 2.22 nm^{-1}, which is estimated for manganites in Ref. [23], (ii) small polaron hopping model (SPH) in $T > \theta_D/2$. This model was utilized to explain the small polaron influence in the conductivity mechanism, which is described by polaron models either adiabatic $\rho = \rho_0 T \exp(E_p/k_B T)$ or non-adiabatic $\rho = T^{3/2} \exp(E_p/k_B T)$ [23], (iii) the thermally activated hopping model. It is describe by equation $\rho = \rho_0 \exp(E_a/k_B T)$, where E_a is the activation energy in semiconducting region [24]. It is hard to tell which of the three models explains the electrical transport properties better at high temperature ($T > T_{MI}$). So, we tried to fit experimental data of $\rho - T$ by using these models to find best fitted model as compared with others. In our case, the small polaron hopping model and adiabatic small polaron model gives the best fit to the experimental data.

Fig. 6 shows typical plots of $\ln(\sigma)$ versus $T^{-1/4}$. The estimated values of T_0 and $N(E_F)$ both in the presence and in the absence of magnetic field are given in Table 1. $(T_0)^{1/4}$ values is utilized to calculate the density of the states at the Fermi level and results are also given in Table 1.

As we can see in Table 1, T_0 increases with x and for a given sample T_0 decreases with the application of the magnetic field, so it is observed that $N(E_F)$ increases with the application of the magnetic field. The increase of $N(E_F)$ with the application of the magnetic field may be due to the suppression of the magnetic domain scattering by the magnetic field. However, its increase is not compared with at zero field. The density of states is found to two to three orders of magnitude higher than those of usual oxide semiconductors. Jung [25] believed that large value of $N(E_F)$ is due to the effect of adiabatic small polaron hopping process. For this reason, the large magnitude of $N(E_F)$ such as $\sim 10^{20}$ affirms the clear signatures of the applicability of the adiabatic hopping model. Therefore, the adiabatic small polaron hopping model is used in the present investigation rather than non-adiabatic small polaron hopping model. Polaron activation energy (E_p) estimated
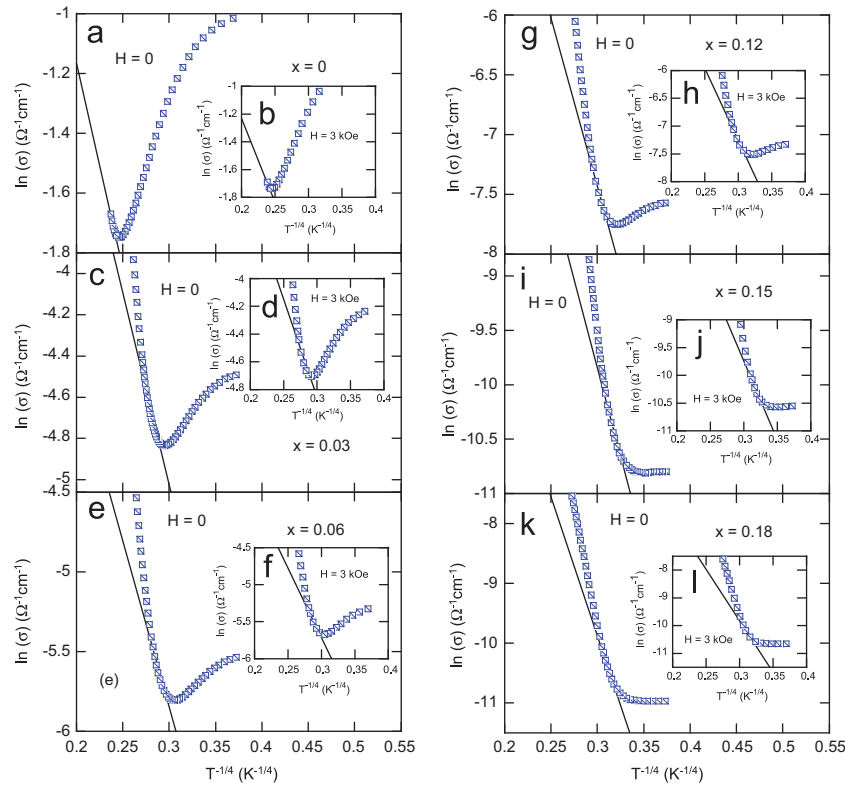

Fig. 6. Plots of $\ln(\sigma)$ vs. $T^{-1/4}$ fitted to $\sigma(T) = \sigma_0 \exp(-T_0/T)^{1/4}$ between T_{MI} and $\theta_D/2$ for the LSMO/BTO composites with $x=0$ (a) and (b); $x=0.03$ (c) and (d); $x=0.06$ (e) and (f), $x=0.12$ (g) and (h), $x=0.15$ (i) and (j); $x=0.18$ (k) and (l). The inset curves (b), (d), (f), (h), (j) and (l) represent the data taken in applied field $H=3$ kOe.

Table 1
Fitting parameters obtained by using different models for LSMO/BTO composites above T_{MI}.

x	$T_0 \times 10^5$ (K)		$N(E_F)$ (eV^{-1}cm^{-3})		E_p (meV)		E_a (meV)		θ_D (K)	ν_{ph} ($\times 10^{12}$ Hz)
	$H=0$	$H=3$ kOe	$H=0$	$H=3$ kOe	$H=0$	$H=3$ kOe	$H=0$	$H=3$ kOe	$H=0$	$H=0$
0.00	0.35	0.27	5.80×10^{22}	7.52×10^{22}	41.45	37.92	30.94	25.85	638	13.29
0.03	1.18	0.40	1.72×10^{22}	5.08×10^{22}	102.03	101.25	101.16	97.98	377	7.85
0.06	1.88	1.24	1.08×10^{22}	1.64×10^{22}	108.14	102.46	109.35	103.83	326	6.79
0.12	6.20	4.40	3.28×10^{21}	4.62×10^{21}	119.52	115.90	113.57	107.11	265	5.52
0.15	10.07	6.76	1.90×10^{21}	3.01×10^{21}	125.64	122.71	115.98	113.49	222	4.63
0.18	12.36	7.13	1.64×10^{21}	2.85×10^{21}	131.50	129.26	77.98	76.35	217	4.52

from fitted curves in Fig. 7 is also given in Table 1. The polaron activation energies increase with the increase of BTO concentration. Table 1 clearly shows that the E_p decreases with the application of the magnetic field and the observed behavior may be attributed to the decrease in the values of charge localization under the influence of the magnetic field [21]. This also indicates that the ferromagnetic coupling of magnetic moments of the neighboring grains in composites is decreased as a result of the introduction of BTO. The ferroelectric BTO in the composites can reduce the carrier concentration at the neighboring LSMO grain boundary. Thus, the resistance increases with increasing BTO addition as described above. This gives equivalent effects to the increase in the activation energy of E_p in the transport process of the carriers. So the results of E_p are reasonable.

Fig. 8 shows the $\rho - T$ data above temperature $T > T_{MI}$ fitted using the thermal activation energy law, $\rho = \rho_0 \exp(E_a/k_B T)$, where E_a is the activation energy in semiconducting region. The deduced activation energy or band gap energy is given in Table 1. From Table 1 it can be found that both polaron activation energy (E_p) and thermal activation energy (E_a) are increasing with increase of the BTO concentration. The increase of the E_p and E_a values may be due to the lattice distortion. N_{ph} (the optical phonon frequencies) were obtained from the relation $h\nu_{ph} = k_B \theta_D$. Both phonon frequency and $\theta_D/2$ decrease against BTO concentration. This indicates that the frequency of lattice wave decreases when there is an increase in the BTO content. It seems that the values of $\theta_D/2$ are much higher than T_{MI}, which highlights the width of VRH region between $\theta_D/2$ and T_{MI} [24].

As mentioned above, the increase of T_0 and the decrease of $N(E_F)$ with the increasing of BTO concentration (Table 1) leads to the increase of the E_p and E_a. In fact, since the BTO act as barriers

to the charge carriers, the e_g electrons of Mn^{3+} ions become localized when BTO is added on the grain boundary. This causes the increase of E_p and E_a. This indicates that disorder plays a key role in the high temperature ($T > T_{MI}$) conduction process, that is, the conduction mechanism in the high temperature is dominated by variable range hopping mechanism and the adiabatic small polaron hopping mechanism. Thus, all the results, including the increase in T_0 and the polaron activation energy (E_p) and the decrease in the density of states at the Fermi level with the BTO content, support that the conduction in LSMO/BTO composites obey to the variable range hopping between localized states.

The magnetic field dependence of the MR for all the samples studied at a fixed temperature 30 K (Fig. 9a) and 300 K (Fig. 9b) measured in the magnetic field range of 0–3 kOe is shown in Fig. 9. The MR ratio is defined as MR (%)=$[\rho(0, T) - \rho(H, T)]/\rho(H, T) \times 100\%$, where $\rho(0, T)$ and $\rho(H, T)$ are the resistivity values for zero and applied fields $H = 3$ kOe, respectively. Fig. 9 indicates that the change in MR is greater in the doped composites as compared to pure LSMO, which indicates that the enhancement in MR basically comes through the formation of composites. The values of the MR at 30 K are about, 22.11%, 22.83%, 23.13%, 24,02%, and 24.63% for x=0.03, 0.06, 0.12, 0.15 and 0.18 respectively while they are about 21.21%, for x=0 at 3 kOe. As mentioned above, one might invoke the role of spin polarized tunneling at the grain boundaries in order to explain the enhancement of MR. Hwang et al. [2] suggested that in polycrystalline samples the main contribution comes from the spin-polarized tunneling between the grains and MR at low fields appears from the magnetic domain rotation at the grain boundaries. However, the magnetic field dependence of the MR at room temperature is different from that at 30 K as shown in Fig. 9b. The magnetic field dependent MR curve at 30 K (Fig. 9a) clearly indicates a sharp enhancement in MR at low fields and a saturation at higher fields,
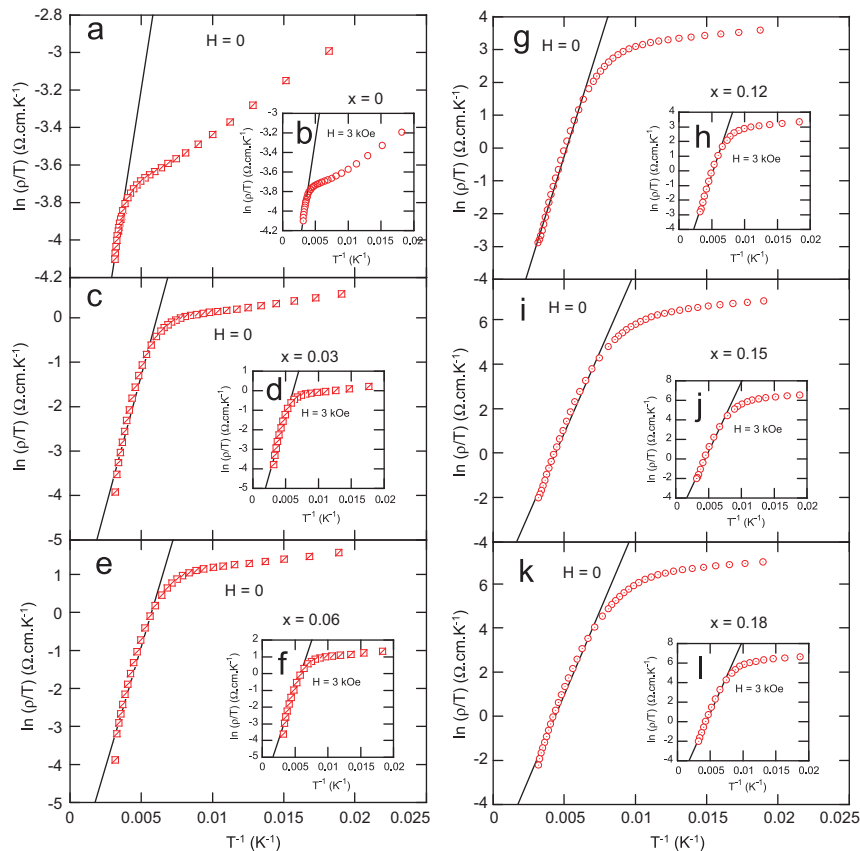

Fig. 7. Fitted curves of ρ vs. T^{-1} for $\rho(T) = \rho_0 T \exp(E_p/k_B T)$ equation above T_{MI} for the composites LSMO/BTO with x=0 (a) and (b); x=0.03 (c) and (d); x=0.06 (e) and (f), x=0.12 (g) and (h), x=0.15 (i) and (j); x=0.18 (k) and (l). The inset curves (b), (d), (f), (h), (j) and (l) are taken in presence of applied field H=3 kOe.
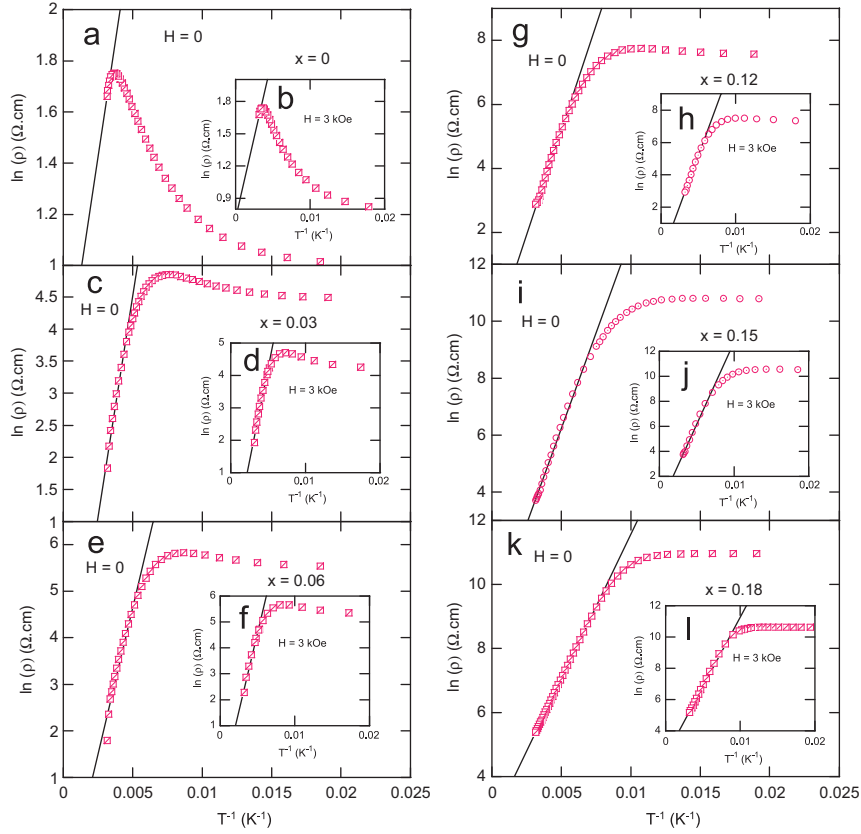
Fig. 8. Fitted curves of ρ vs. T^{-1} for $\rho(T) = \rho_0 \exp(E_a/k_B T)$ equation above T_{MI} for the composites LSMO/BTO with $x=0$ (a) and (b); $x=0.03$ (c) and (d); $x=0.06$ (e) and (f), $x=0.12$ (g) and (h), $x=0.15$ (i) and (j); $x=0.18$ (k) and (l). The inset curves (b), (d), (f), (h), (j) and (l) are taken in presence of applied field $H=3$kOe.
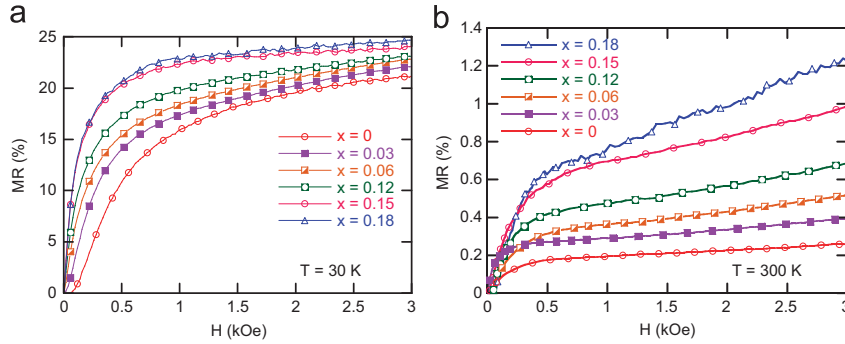

Fig. 9. Magnetic field dependence of the magnetoresistance (MR) in a magnetic field (0–3 kOe) at 30 K (a) and 300 K (b) for the composites LSMO/BTO.

while at room temperature the MR increases with field almost linearly, except $H < 0.5$ kOe (Fig. 9b), which is high field magnetoresistance (HFMR) behavior. This HFMR originates from the ordering of grain boundary spins and provides information about the magnetic behavior of grain boundary regions [11,26]. In our case, this HFMR increases with increasing BTO concentration in the composite samples and is maximum for the composite with $x=0.18$ and hence these results suggest that the materials used in our studies are useful for a real application.

In order to study LFMR behavior, we utilized phenomenological model of Roy and Das [27]. According to this model, the total MR can be written as the sum of grain boundary contribution and the intragrain contribution as: $MR = MR_{GB} + MR_{grain}$. In zero field, the domain walls are pinned at the grain boundaries, which act as the pinning centers with pinning field h_p. The pinning field is defined as the minimum field needed to overcome a particular pinning barrier and has the distribution. Therefore, total MR is

expressed as

$$MR = -A_0 \int_0^H f(h_p) dh_p - A_3 H - A_3 - A_4 H^3 \qquad (1)$$

where $A_0 = N\partial r/R_0, \partial r$ is the drop of resistivity due to the slippage of the domain boundary from the grain boundary, N is the number of domain walls in the grain boundaries and R_0 is zero field resistivity. The first term in (1) is the contribution from spin polarized tunneling (MR_{GB}) and the other two terms represent the intrinsic contribution from Zener double exchange (MR_{grain}). Both A_3 and A_4 are constants.

Since the distribution of pinning field can be assumed as Gaussian $f(h_p) x \exp(-A_2^2 h_2^2)$ (A_2 is constant) in nature, the MR can be written as

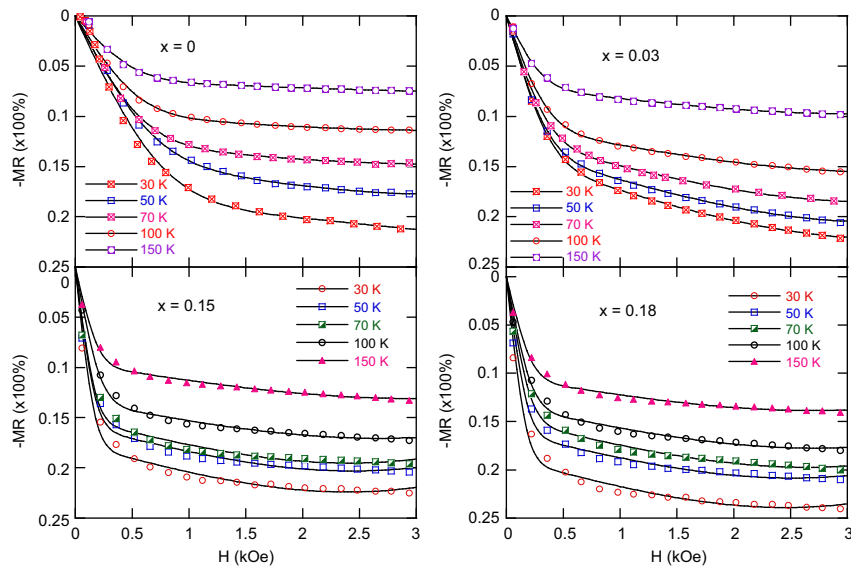$$MR_{total} = -A_3 H - A_4 H - A_1 erf(A_2 H) \qquad (2)$$

Fig. 10. Experimental MR vs. *H* curve (dot) at various temperature in the magnetic field range of 0–3 kOe for samples with $x=0$; 0.03; 0.15 and 0.18 and the fitted curve (line) using Eq. (2).

where

$$A1 = \sqrt{\pi}A_0/2A_2$$

The experimental MR(*H*) data were fitted with Eq. (2) and the results are represented in Fig. 10. It is evident that the theoretical curves fit very well with the experimental data. As temperature increase, the coefficients A_1 and A_2, which are related with MR_{GB}, decrease, whereas the coefficients A_3 and A_4, related with MR_{grain}, increase.

4. Conclusions

In conclusion, we have fabricated and studied the effect of BTO in LSMO/BTO composites. The electrical properties of pure LSMO are significantly modified by introducing the ferroelectric BTO. With increasing BTO content, the Curie temperature remains a constant at about 357 K, the metal-insulator transition temperature decreases from 295 K for $x=0$ to 51 K for the sample with $x=0.18$, simultaneity the resistivity of the composites increases. We analyzed the resistivity of composites in the paramagnetic insulating regime by different existing models. Decrease in the density of states (and the decrease in the T_0) obtained through Mott's variable range hopping mechanism is attributed to the suppression of magnetic domain scattering with applied field and BTO. Furthermore, from the present study, it can be concluded that the polaron activation energy increasing with increase of BTO concentration. Finally, it has also been concluded that the adiabatic small polaron hopping mechanism and variable range hopping mechanism can be used to interpret the electronic transport properties in the high temperature $(T > T_{MI})$ regime. The observed LFMR of the polycrystalline samples is dominated by the spin-polarized tunneling effect between the grains. This effect becomes more important at room temperature as compared to that of pure LSMO manganites.

References

[1] C. Zener, Phys. Rev. 82 (1951) 403.
[2] H.Y. Hwang, S.W. Cheong, N.P. Ong, B. Batlogg, Phys. Rev. Lett. 77 (1996) 2041.
[3] A. Gupta, J.S. Sun, J. Magn. Magn. Mater. 200 (1999) 24.
[4] A. Gaur, G.D. Varma, J. Alloys Compd. 453 (2008) 423.
[5] P.T. Phong, N.V. Dai, D.H Manh, N.V. Khiem, L.V. Hong, N.X. Phuc, J. Alloys Compd. 485 (2009) L39.
[6] P.T. Phong, N.V. Khiem, N.V. Dai, D.H. Manh, L.V. Hong, N.X. Phuc, J. Magn. Magn. Mater. 200 (2009) 3330.
[7] P.T. Phong, N.V. Khiem, N.V. Dai, D.H. Manh, L.V. Hong, N.X. Phuc, Mater. Lett. 63 (2009) 353.
[8] J.H. Miao, S.L. Yuan, L. Yuan, G.M. Ren, X. Xiao, G.Q. Yu, Y.Q. Wang, S.Y. Yin, Mater. Res. Bull. 43 (2008) 631.
[9] M. Eshraghi, H. Salamati, P. Kameli, J. Alloys Compd. 437 (2007) 22.
[10] Chang Seop Hong, Wan Seop Kim, Nam Hwi Hur, Solid State Commun. 121 (2002) 657.
[11] A. Gaur, G.D. Varma, Solid State Commun. 139 (2006) 310.
[12] N.V. Khiem, P.T. Phong, N.V. Dai, D.H. Manh, L.V. Hong, N.X. Phuc, Mater. Lett. 63 (2009) 899.
[13] V.P.S. Awana, Rahul Tripathi, S. Balamurugan, H. Kishan, E. Takayama-Muromachi, Solid State Commun. 140 (2006) 410.
[14] P.T. Phong, N.V. Khiem, N.V. Dai, D.H. Manh, L.V. Hong, N.X. Phuc, J. Alloys Compd. 484 (2009) 12.
[15] Yuan Xiao-Bo, Liu Yi-Hua, Wang Cheng-Jian, Mei Liang-Mo, Appl. Phys. Lett. 88 (2006) 042508.
[16] Bose Esa, S. Tarana, S. Karmakara, B.K. Chaudhuri, S. Pal, C.P. Sun, H.D. Yang, J. Magn. Magn. Mater. 314 (2007) 30.
[17] Sunita Keshri (Shaw), Leena Joshi, Sanjeeb Kumar Rout, J. Alloys Compd. 485 (2009) 501.
[18] G.M. Ren, S.L. Yuan, H.G. Guan, X. Xiao, G.Q. Yu, J.H. Miao, Y.Q. Wang, S.Y. Yin, Mater. Lett. 61 (2007) 767.
[19] A de Andres, M Garcia-Hernandez, J.L Martinez, Phys. Rev. B 60 (1999) 7328.
[20] J.M. Rubinstein, J. Appl. Phys. 87 (2000) 5019.
[21] S. Bhattacharya, R.K. Mukherjee, B.K. Chaudhuri, H.D. Yang, Appl. Phys. Lett. 82 (2003) 4101.
[22] N.V. Khiem, L.V. Bau, L.H. Son, N.X. Phuc, D.N.H. Nam, J. Magn. Magn. Mater. 262 (2003) 490.
[23] A. Banerjee, S. Pal, B.K. Chaudhuri, J. Chem. Phys. 115 (2001) 1550.
[24] E. Tka, K. Cherif, J. Dhahri, E. Dhahri, J. Alloys Compd. 509 (2011) 8047.
[25] W.H. Jung, J. Mater. Sci. Lett. 17 (1998) 1317.
[26] R.B. Gangineni, K. Dorr, N. Kozlova, K. Nenkov, K.H. Muller, L. Schultz, L.Seetha Lakshmi, J. Appl. Phys. 99 (2006) 053904.
[27] B. Roy, S. Das, J. Appl. Phys. 104 (2008) 103915.